N82 23424

Acoustically Induced Oscillation and Rotation of a Large Drop in Space

Nathan Jacobi, Arvid P. Croonquist, Daniel D. Elleman, and Taylor G. Wang

Jet Propulsion Laboratory, California Institute of Technology
Pasadena, California 91109

Abstract

A 2.5 cm diameter water drop was successfully deployed and manipulated in a triaxial acoustic resonance chamber during a 240 sec low-gravity SPAR rocket flight. Oscillation and rotation were induced by modulating and phase shifting the signals to the speakers. Portions of the film record were digitized and analyzed. Spectral analysis brought out the n = 2, 3 4 free oscillation modes of the drop, its very low-frequency center-of-mass motion in the acoustic potential well, and the forced oscillation frequency. The drop boundaries were least-square fitted to general ellipses, providing eccentricities of the distorted drop. The normalized equatorial area of the rotating drop was plotted vs a rotational parameter, and was in excellent agreement with values derived from the theory of equilibrium shapes of rotating liquid drops.

Introduction

This report describes an experimental study which is contributing to the understanding of containerless processing of molten materials in space. This study was performed on a 2.5 cm diameter water drop successfully deployed and manipulated in a triaxial acoustic resonance chamber during a 5 min SPAR (Space Processing Applications Rocket) flight. Three aspects of containerless processing technology in space are of particular interest: stability, oscillation, and rotation of a molten sample. Stability studies will help us determine the effect of residual g-jitter on the positioned sample, as well as the focusing requirement of the optics. Oscillation studies will enable us to measure the surface tension of the sample, as well as to better understand induced mixing currents within a liquid melt. Rotation studies will demonstrate the feasibility of degassing and shaping melts. In addition, a rotating sample can even out the nonuniformity of the temperature environment.

With these broad objectives in mind, the primary objectives of this flight were to: (1) Study the center-of-mass motion in an acoustic chamber. The initial velocity and position of the drop due to the retraction of the injectors gave the drop energy to oscillate in the acoustic potential well throughout most of the experiment. Effects of g-jitter on this motion can be observed from the film record and accelerometer telemetry. (2) Determine the rotation capability of the acoustic chamber. The torque on the drop generated by the acoustic field slowly rotates the drop up to 2 rps. The rate of spin-up establishes the rotation capability of the chamber on a liquid drop. (3) Study the drop shape change due to rotation. The shapes of the drop in near rigid-body rotation from this experiment are compared with existing equilibrium shape calculations. If rotation is to be used as a method of shaping liquid melts, it is important to determine the deviation between calculated and observed shapes. (4) Study the frequency response and damping mechanisms of drop oscillations for both free and forced oscillations. The initial perturbation of the drop shape generated by the drop injection system is allowed to damp down with the acoustic field on. The time required for the positioned liquid drop to approach its quiescent state can be determined from the film record.

Apparatus and Operation

A schematic drawing of the payload is shown in Fig. 1. The heart of the apparatus is a triaxial acoustic resonance chamber which is used to position and control large liquid drops in low-g environments. The chamber itself is nearly cubical, with inside dimensions of 11.43 x 11.43 x 12.70 cm. Three acoustic drivers are fixed rigidly to the center of three mutually perpendicular faces of the chamber. During operation of the chamber, each driver excites the lowest-order standing wave along the direction that it faces. In the resonant mode, the acoustic pressure is maximum at the nodes of the velocity wave (i.e., at the walls) and minimum at the antinodes (the center). There is a tendency for introduced liquids and particles to be driven toward the antinodes, where they collect and remain until excitation ceases.

Rotation of the sample requires that two dimensions of the chamber, the x and y, be of the same length and that the x and y drivers be driven at the same frequency with a phase separation of 90°. For non-rotation applications, the two axes can be driven at 0° or 180° with respect to one another. However, at these phase shifts, interference patterns

are produced in the chamber that seriously distort the shape of the drop. In order to alleviate this problem, the acoustic fields are turned on and off in a cyclic manner so that when the x axis acoustic field is on the y acoustic field is off, and when the x is off the y is on. This complementary modulation of the x and y axes is done at a frequency that is high compared to the frequencies of the lowest normal modes of the drop.

The acoustic chamber was located in the rocket payload so that the z axis of the chamber was parallel to the center line of the rocket (Fig. 1). The bulk of the data from this experiment was obtained with a 16 mm cine camera, run at 48 frames per second. The camera was directed along the z axis ; in addition, two mirrors gave nearby orthogonal views along the x and y axes. The sound intensity at each wall, the deployment system condition, camera and lighting status, and the frequency of the z-axis signal were monitored, telemetered to the ground station and recorded in real time.

This type of acoustic resonance chamber was designed by Wang et al.[1] for levitation and space processing applications. More details and the results of analysis of a previous SPAR flight can be found in Jacobi et al.[2]

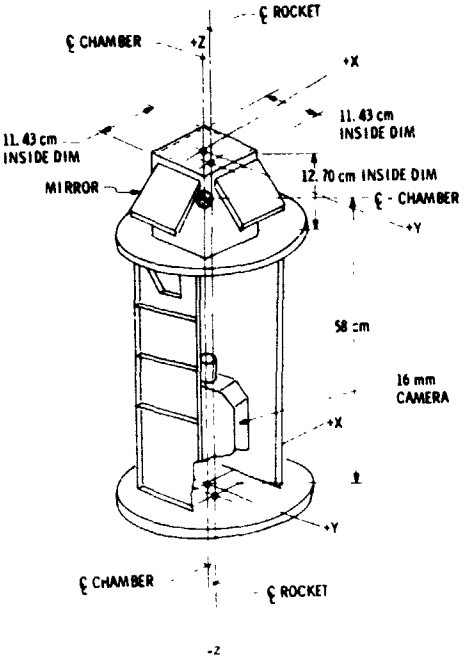

Fig. 1. Schematic drawing of the SPAR payload showing the acoustic chamber, cine camera, and mirrors.

Data Analysis

The timing for the various phases of this flight experiment is presented in Table 1. The following five time sequences were identified for analysis.

(a) Free oscillation (127-145 sec). When the fluid injectors were retracted, the drop was held in position by the acoustic field. Free oscillations (excited by the retracting injectors) damped out, and the drop moved back and forth in the acoustic potential well. This part was used to observe free oscillations, to measure the radius of the drop, and to study its center-of-mass motion.

Table 1. Sequence of Events

Clock Time (sec after lift-off)	Event
85	Camera on
90	Complementary modulation on
105	Fluid delivered through injector
117	Fluid delivery off
127	Fluid injectors extracted
127-145	Free oscillation
145	z modulation on
145-265	Forced oscillation
265	z modulation off
265-300	Drop relaxation
300	Complementary modulation off; 90 phase shift
300-330	Induced rotation
330	90° phase shift off; complementary modulation on
330-360	Coasting
365.5	Drop hits wall

(b) Forced oscillation (145-147 sec). As the acoustic pressure along the z axis was modulated at a low frequency, the resulting oscillatons of the drop were very regular for three seconds.

(c) Combined oscillation and rotation (147-265 sec). The regular behavior of the drop's response to the z axis modulation quickly developed an unexpected twist: to the large amplitude oscillation was added rotation of the drop. This sequence is the most difficult and intriguing one to interpret. The acoustic forces and torques on a strongly deformed drop at an arbitrary position are poorly understood.

(d) Relaxation of the drop (265-300 sec). With the complementary modulation of the x and y axes on, the drop relaxed prior to being spun up. The information in this sequence was similar to that in sequence (a).

(e) Spin-up of the drop (300-330 sec). With a phase difference of 90° between the x and y pressure amplitudes, a torque was generated on the drop which caused it to rotate the z axis. Deformed shapes were observed, which can be compared with theoretical predictions of the equilibrium shape of a rotating liquid drop.

The strategy used for the data analysis of the 16 mm cine film record consisted of preliminary analysis performed on a Vanguard Motion Film Analyzer and a more detailed study of fully-digitized boundaries of selected frames (provided by JPL's Image Processing Laboratory) using a small computer. A sample cine frame is shown in Fig. 2a, from the forced oscillation sequence. Figure 2b shows the computer-digitized boundaries for the frame in the preceding photograph. Both the "raw" data and a quadratically-smoothed boundary are shown for each of the three views. It must be noted that, despite the satisfactory appearance of the original photograph, some irregularities do appear in the digitized and smoothed versions. These may be due to overlap with the speaker ports, specular or back reflections, or to a peculiarity in the digitization algorithm. It is a persistent feature throughout the film. Table 2 shows the frame sequences that were digitized and the frame densities. The total number of frames processed was 1826, with typically 90 to 150 points per boundary. The boundary data were recorded in the form of 3-digit integers, thus placing a limit upon the resolution of the digitization.

Fig. 2a. Typical frame from the 16 mm record which shows three orthogonal views of the drop undergoing forced oscillation (t = 147.0 sec).

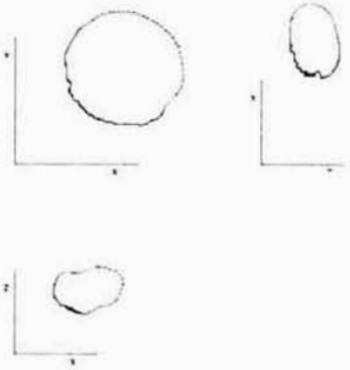

Fig. 2b. Digitized boundaries of the drop images shown in a. The points are "raw" data and the lines are their quadratically-smoothed description.

Table 2. Digitized Frames

Time (sec)	Event	Density
127.1--130.4	Free oscillation	1/1
130.4--144.6	Free oscillation	1/3
144.6--147.1	Forced response: regular	1/1
147.1--170.4	Forced response: rotation	1/3
263.7--300.4	Free oscillation	1/4
300.4--333.7	Rotation	1/5

It was felt that prior to the automatic processing of relatively large amounts of data, it would be useful to investigate some of the interesting features on a Vanguard

Motion Film Analyzer. These measurements provided some insight into what might be expected from a more detailed analysis. Three topics were handled with this simple technique. As the drop moved periodically in the acoustic potential well, the frequency of the motion was measured and compared with a theoretical prediction approximating the acoustic potential well by an equivalent harmonic oscillator potential. These frequencies are correlated with the acoustic force and with the pressure level in the chamber. The two lowest normal mode frequencies, f_2 and f_3, were identified. With a knowledge of the surface tension, measured shortly before the flight, these measurements were used to infer the volume of the drop. The ratio of the minor to major axes was measured before, during, and after the rotation sequence. While there was significant scatter in the results, the ratio was close to 1.0 prior to rotation, and showed a measurable change when the drop was spun up.

While some of the main results will be described on the following pages, more details concerning the analysis of this flight can be found in the report by Wang et al.[3]

Numerical tests. As another preparatory step to the data analysis, it was decided to investigate numerical test cases involving the recovery of a known signal in the presence of various amounts of noise. The first of two such experiments was designed to recover the coefficients of the normal modes of a perturbed boundary, a situation which is encountered when analyzing the oscillatory motion of a drop. The boundary was represented in the form

$$\frac{r(\theta)}{R} = 1 + \sum_n a_n P_n(\cos\theta) + bN \quad , \tag{1}$$

where a_n are preassigned values, and b is the noise amplitude. The problem was to recover a_n in the presence of noise, by either direct numerical integration around the boundary, using the orthogonality of the Legendre polynomials, or by least squares techniques which avoided the approximation involved in numerical integration. The results were similar for both approaches, with somewhat better accuracy provided by the least squares analysis.

The second numerical experiment was designed to determine the ratio of the major to minor axis of a general perturbed ellipse, a situation encountered when a drop is distorted either by rotation or oscillation. In this case the coefficients of a general ellipse

$$ax^2 + 2bxy + cy^2 + 2dx + 2ey + 1 = 0 \tag{2}$$

in the presence of noise, were determined by a least squares approach. The coefficients a, b, c determine the principal axis of the ellipse

$$\text{tg } 2\alpha = \frac{2b}{a - c} \tag{3}$$

and the ratio of axes is given by

$$\text{ratio} = \left(\frac{a\sin^2\alpha + c\cos^2\alpha - b\sin 2\alpha}{a\cos^2\alpha + c\sin^2\alpha + b\sin 2\alpha}\right)^{\frac{1}{2}} \tag{4}$$

This ratio was also determined by a direct "min-max" approach, where extremal radius vectors from an approximate center are found. This approach was found to be noise-limited, and impractical for useful data reduction.

Center-of-Mass Motion

A large water drop moves in an acoustic potential well determined by the acoustic force components

$$F_i = \frac{5\pi}{6}\frac{p_i^2}{\rho_a c^2}\, k_i a^3 f(2k_i a)\sin 2k_i x_i \tag{5}$$

where p is the acoustic pressure, ρ_a is the density of air, c is the speed of sound, $k_i = \pi/L_i$ is the wave number, and $f(2k_ia)$ is a shape factor

$$f(2k_ia) = \frac{\frac{\sin 2k_ia}{2k_ia} - \cos 2k_ia}{\frac{1}{3}(2k_ia)^3} \xrightarrow[k_ia \to 0]{} 1 - \frac{1}{10}(2k_ia)^2 \tag{6}$$

This expression for the force was recently verified by laboratory measurements and analysis by Leung et al.[4] For small displacements from the center $\sin 2k_ix_i \sim 2k_ix_i$, resulting in a harmonic oscillator well in which the frequency of oscillation will be

$$\omega_{cm}^2 = \frac{5}{4} f(2k_ia) \frac{k_i^2 p_i^2}{\rho_d \rho_a c^2} \tag{7}$$

where ρ_d is the drop density.

The oscillation frequency of the center-of-mass motion was determined from the film in two ways. First, the center-of-mass motion was crudely studied on the Vanguard, and a center-of-mass frequency was determined by averaging over several cycles. At 265 sec, the sound pressure level was decreased from 148 to 145 dB, which corresponds to a decrease by a factor of 2 in the force and of $\sqrt{2}$ or 0.71 in the frequency. The corresponding ratios of observed frequencies along the three axes were 0.81, 0.84, and 0.80. Secondly, the center-of-mass coordinates of the digitized boundaries were determined, and then Fourier transformed. A sample is shown in Fig. 3, where (a) shows two periods of the oscillation of one coordinate, and (b) shows the corresponding power spectrum. Typically observed frequencies were ~ 0.15 Hz, while the value predicted from Eq. (7) is ~ 0.14. Because there is a change in elevation between JPL (where the package was calibrated) and White Sands Test Range (where it was sealed prior to launch), there were some changes in the acoustic parameters involved. An estimate showed that the theoretical value of 0.14 Hz should be modified to ~ 0.16 Hz. If the nonharmonicity of the acoustic potential well were taken into account, a reduction of several percent is expected in the value of the center-of-mass frequency.

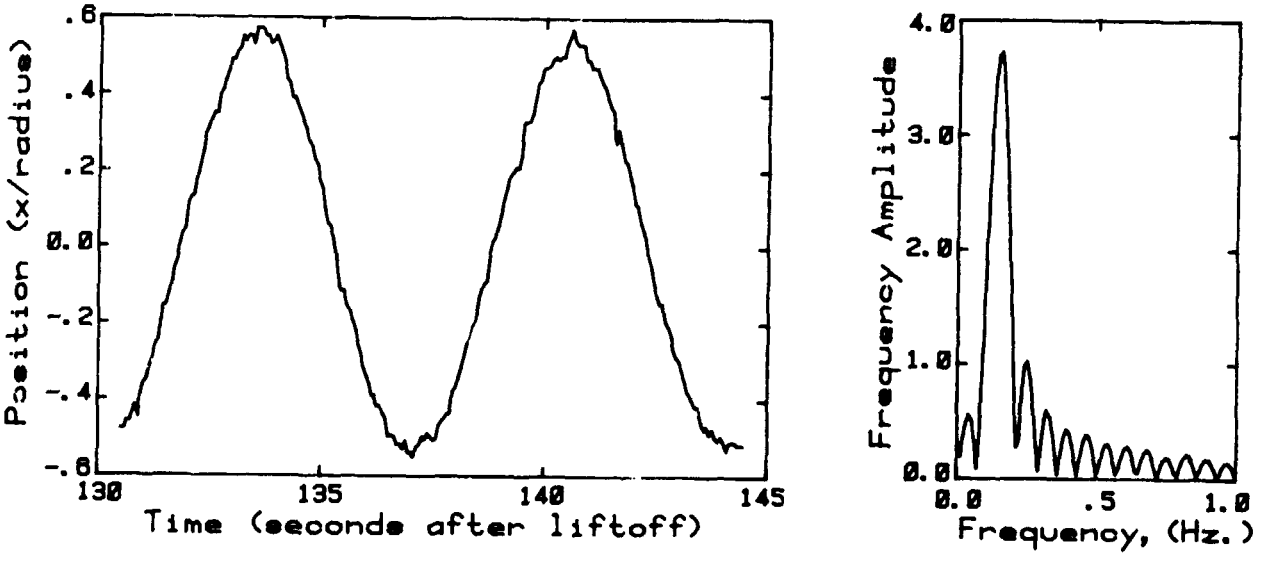

Fig. 3. Study of the center-of-mass motion of the drop in the acoustic potential well:

(a) sinusoidal behavior in the time domain
(b) a single peak in the frequency domain.

Rotation

For the thirty seconds of induced rotation (1600 frames on the film), every fifth frame was digitized. The expectation was that the drop's appearance in the main view, for which the line of view coincided with the axis of rotation, would be circular, while in the side views it would appear circular initially and become gradually more and more

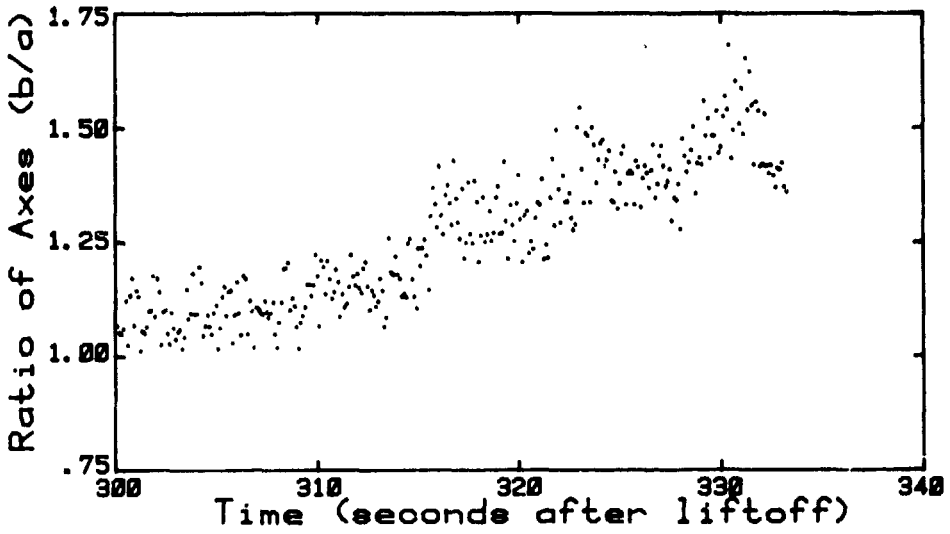

Fig. 4. Ratio of the major and minor axes during the sequence when the acoustic torque was acting on the drop (300 to 330 sec). The view is perpendicular to the axis of rotation. From this ratio a value of Ω was obtained. For example, b/a = 1.5 corresponds to Ω = 0.42.

elliptical. These frames were analyzed by the least squares ellipse analysis (see Eqs. 2-4 above). The expected features showed up.. While the a/b ratio of the main view remained constant, the same ratio for a side view gradually increased from 1.0 at the onset of rotation to roughly 1.5 at the end (Fig. 4). Using the theoretical results of Chandrasekhar[5], Ross[6], and Brown[7], we were able to relate the observed a/b ratio to the rotational parameter

$$\Sigma = \left(\frac{\Omega}{\omega_2}\right)^2 \qquad (8)$$

where Ω is the angular velocity of the rotating drop, and ω_2 is the lowest mode oscillation frequency. The observed a/b ratio at the end of the rotation sequence corresponds to $\Sigma \sim 0.3$. This value, in turn, implies a rotation rate of 8.92 radians/sec, or 1.42 rps. Thus, although we could not directly determine the angular velocity for lack of tracer particles, we were able to infer it using these theoretical relations. Also, note that the value of Σ reached is very close to the first bifurcation point ($\Sigma = 0.313$), at which the theory of equilibrium shapes of a rotating drop predicts possible transition from axially symmetric to non-axially symmetric equilibrium shapes.

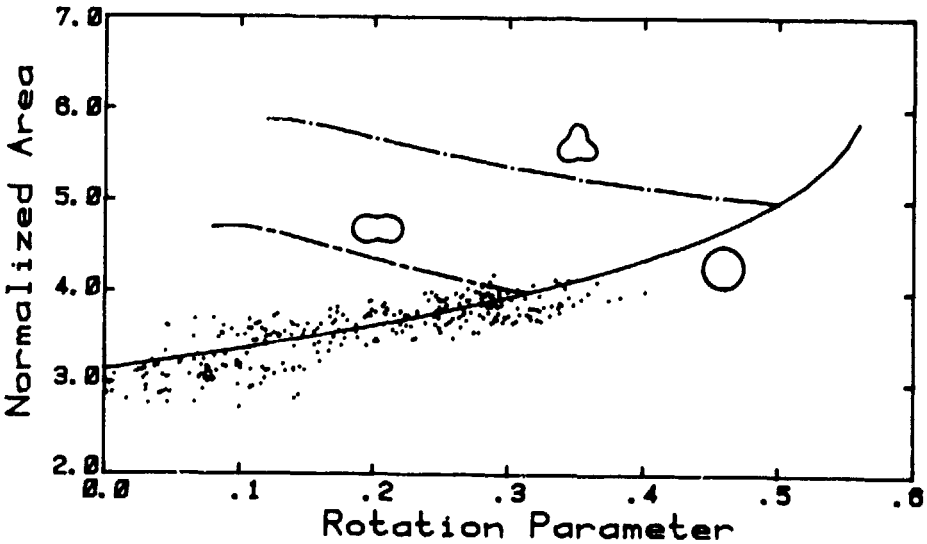

Fig. 5. Comparison of the experimental points and theoretical curves (Brown[7]) relating the equatorial area to the angular velocity. All quantities are normalized: A = Eq. Area/(Resting Radius)^2 and Σ = Rot. Par. = $(\Omega/\omega_2)^2$. The curve through the data represents the axisymmetric family of equilibrium shapes while the two side branches represent two- and three-lobed shapes.

The analysis was continued one more step. A relative equatorial area can be found from the product ab in the main view. A comparison of the theoretical and observed normalized equatorial areas is shown in Fig. 5 in which all boundary points were included in the analysis, showing excellent agreement with the theory. To the best of our knowledge, this is the first time that an observation has been made under conditions similar to those stipulated by the theory of equilibrium shapes of rotating drops. This obviously calls for an extension of such measurements to higher rotation rates. If a drop were spun in one direction and the torque quickly reversed, it might enable observation of the nonaxially symmetric equilibrium shapes theoretically predicted.

Oscillation

The natural oscillation frequencies of a liquid drop are given in the linear approximation by

$$\omega_n^2 = n(n-1)(n+2)\frac{\sigma}{\rho_d a^3} \tag{9}$$

where σ is the surface of the drop. The oscillation frequencies can be determined by analyzing both free oscillation data (as was done in Ref. 2) and forced oscillation data. When the drop oscillated, the reflections of the photo lamps showed that motion; using the time information on the edge of the film and advancing the film through a certain number of cycles, a rough value of the frequency of these oscillations could be obtained. The frequencies $f_2 = 2.48 \pm .03$ and $f_3 = 4.67 \pm .05$ Hz were obtained from the early sequence (127-145 sec) and $f_2 = 2.54 \pm .03$ from the latter (265-300 sec). The frequencies expected for an 8.6 cc water drop with a surface tension of 71 dynes/cm are $f_2 = 2.74$ Hz and $f_3 = 5.31$ Hz. Frequencies were also determined by the peaks of the power spectrum of vertical and horizontal chords on the digitized data. Such a sample is shown in Fig. 6, where the power spectrum shows the mode n = 2, as well as traces of the modes n = 3, 4. At the time of this writing the full boundaries are being analyzed to provide the coefficients $a_n(t)$ of Eq. (1). The Fourier transform of the latter is expected to provide the corresponding frequencies.

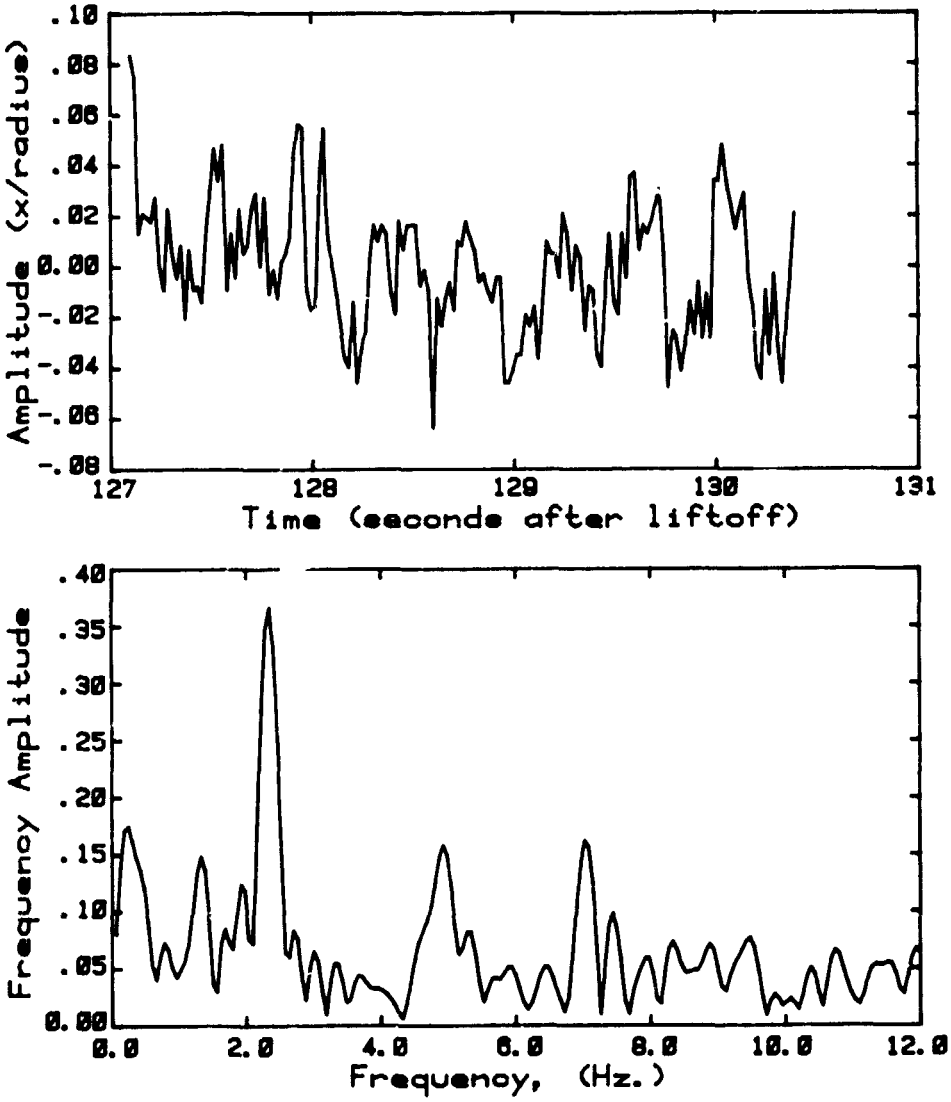

Fig. 6. Study of the drop's natural oscillations:
(a) difference between vertical and horizontal oscillations.
(b) frequency spectrum of data shown in (a).

During the forced oscillation sequence, the amplitude modulation of the acoustic pressure field along the z axis was swept from 2.3 to 2.9 Hz over a two-minute period, so as to contain the expected resonant frequency, 2.6 Hz, with a sufficient safety margin. The drop began oscillating in the n = 2 normal mode during the first few seconds, as intended. However, as the amplitude became very large, the regularity deteriorated ver quickly and rotation set in. The coefficient $a_2(t)$ in Eq. (1) was determined by direct numerical integration, and by a vertical-horizontal chord method. The results are described in Ref. 3, but it can be generally stated that the cause of the rotational stability which developd two seconds into the forced oscillation sequence is not well understood at the present time. The acoustic field in which the drop finds itself is fairly complicated. Its components along each axis are modulated: there was amplitude modulation along the z axis, and complementary modulation along the x and y axes. In addition, the drop was undergoing a continuous low-frequency center-of-mass motion in this complex potential field.

Conclusions

The objectives of this experiment were achieved. The drop was deployed and acoustically manipulated as planned.

There is no satisfactory understanding of the intially strong oscillation seen during the forced oscillation sequence (at 2.3 Hz rather than 2.5 Hz) and the subsequent highly irregular motion which appears to be a superposition of oscillation and rotation.

During the rotation sequence of this experiment, the first bifurcation point between axisymmetric and triaxial shapes was reached in only thirty seconds of applied torque. Since equilibrium probably had not been reached, this means that spending more time on the rotation sequence or increasing the torque by using a higher sound pressure in future experiments might take the drop beyond the first bifurcation point. In particular, such an experiment would show whether non-axially symmetric equilibrium shapes are excited beyond the first bifurcation point.

Acknowledgements

The authors are grateful to P. Rayermann and J. Brown for assistance in data processing and programming; to R. Selzer and R. Ramage of the Image Processing Laboratory at JPL for digitizing the data; and to R. Irigoyen, J. Conley, L. Robinson, and K. Tarver for their valuable assistance in all phases of this experiment. This paper presents the results of one phase of research carried out at the Jet Propulsion Laboratory, California Institute of Technology, under contract with the National Aeronautics and Space Administration.

References

1. T. G. Wang, M. M. Saffren, and D. D. Elleman, Acoustic Chamber for Space Processing, AIAA paper 74-155 (1974).

2. N. Jacobi, R. P. Tagg, J. M. Kendall, D. D. Elleman, and T. G. Wang, Free Oscillations of a Large Drop in Space, AIAA paper 79-225 (1979).

3. T. G. Wang, D. D. Elleman, N. Jacobi, and A. P. Croonquist, Containerless Processing Technology Experiment Report, SPAR VI, Experiment 76-20 (May 1981).

4. E. Leung, N. Jacobi, and T. G. Wang, Acoustic Radiation Force on a Rigid Sphere in a Resonance Chamber, JASA, in press (December 1981).

5. S. Chandrasekhar, The stability of a rotating liquid drop, Proc. Roy. Soc. A286, 25 (1965).

6. D. K. Ross, The shape and energy of a revolving liquid mass held together by surface tension, Aust. J. Phys. 21, 823 (1968).

7. R. Brown, The shape and stability of three-dimensional interfaces, Ph.D. thesis, U. of Minnesota (1979).